Orientational Order in Sphere-Forming Block Copolymer Thin Films Aligned under Shear

Andrew P. Marencic,† Mingshaw W. Wu,‡ and Richard A. Register*,†

Departments of Chemical Engineering and Physics, Princeton University, Princeton, New Jersey 08544

Paul M. Chaikin

Department of Physics and Center for Soft Condensed Matter Research, New York, New York 10003

Received June 15, 2007; Revised Manuscript Received July 22, 2007

ABSTRACT: Shear can impart a high degree of orientational order to block copolymer thin films containing two or more layers of spherical domains, but the orientational order appears to plateau at a limited level with increasing shear stress. At high stresses, the only defects which remain in the film are isolated dislocations, and the orientational order in the film is thus uniquely and inversely correlated with the dislocation density. These dislocations preferentially orient normal to the shear direction, which facilitates the sliding of layers of spheres relative to each other during shearing. A simple elastic continuum model provides a good quantitative description of the impact of isolated dislocations on the films' orientational order. At low dislocation densities, the apparent orientational order is limited by uncertainties in locating the positions of the spheres by atomic force microscopy, an effect which is quantitatively captured in this work.

Introduction

Block copolymers have attracted considerable attention for their ability to self-assemble into highly regular morphologies with periodicities of tens of nanometers, where the size and shape of the nanodomains can be controlled easily through the lengths of the constituent blocks.[1,2] Block copolymer thin films are of interest as nanolithographic masks because the fine-scale, dense periodic structures which they form are inaccessible via standard lithographic techniques.[3,4] However, the parallel nature of self-assembly also has an important drawback: upon quenching from the disordered state, block copolymer nanodomains nucleate at random positions and with uncorrelated orientations, leading to a polygrain structure with no global alignment.[5−7] For thin films of block copolymers forming either spherical nanodomains[8−11] or cylinders standing perpendicular to the substrate[12−14] graphoepitaxy can impart orientational order to the domains; graphoepitaxy employs topographic features, such as step edges, along which a particular lattice plane aligns preferentially, such as the (10) plane of the hexagonal macrolattice formed by a single layer of spherical domains. To achieve a single-crystal-type texture by graphoepitaxy over a macroscopic area, a substrate can be patterned with a grid of topographic features spaced by less than the grain size of the block copolymer, typically a few micrometers or less.[15]

An alternative approach to orient spherical nanodomains over macroscopic areas, without requiring prepatterned substrates, is to shear the block copolymer film parallel to the substrate.[16−19] Alignment can be achieved with a few minutes of shearing, over cm^2 regions of film, and with stresses (order 1000 Pa) small enough that they can be imparted by either a moving solid surface in contact with the film[16,17] or simply a fluid flowing over the film's surface.[18,19] However, the alignment induced by shear is not perfect: some defects (mostly dislocations) remain in the sheared films, which limit the translational order to short range (comparable to the distance between dislocations) and reduce the quality of the orientational order, though the latter remains long range (set by the dimension of the sheared area). Here, we discuss the factors that limit the measured orientational order of sphere-forming block copolymer thin films aligned under shear.

* To whom correspondence should be addressed. E-mail: register@princeton.edu.
† Department of Chemical Engineering, Princeton University.
‡ Department of Physics, Princeton University.

Experimental Section

Materials. The polystyrene-block-poly(ethylene-alt-propylene) (PS-PEP) diblock employed here is identical to that employed in our previous studies.[17,18] It was synthesized through sequential living anionic polymerization[20] followed by hydrogenation;[21] number-average block molecular weights are 3.3 kg/mol for PS and 23.1 kg/mol for PEP. Small-angle X-ray scattering (SAXS) on bulk samples confirmed the expected morphology of spheres packed on a body-centered cubic (bcc) lattice with an order−disorder transition temperature[20] (T_{ODT}) of 121 ± 2 °C. In a thin film, the minority PS block forms a brush-like wetting layer on the silicon wafer substrate (used as purchased from Silicon Quest International) on top of which form layers of hexagonally packed PS spheres within a PEP matrix.[17] This hexagonal packing persists at least up to the three-layer films studied in this work, though a reconstruction toward the bulk bcc structure is eventually expected as film thickness is increased.[22]

Sample Preparation. PS-PEP was applied to the silicon wafers by spin coating from a dilute solution (∼1−2% by weight). By adjusting the spin speed and concentration, the number of layers of spheres could be controlled. A monolayer of spheres does not shear align due to its lack of mechanical anisotropy.[17] All the data presented here correspond to three layers of spheres (78 nm total film thickness), though more limited studies with simple two-layer films showed no discernible differences from the three-layer films. No terracing (islands or holes) was visible in any of the films before or after shearing. Shear is applied to the thin film in a constant-stress rheometer (Rheometrics DSR-200 or Anton Paar MCR-501). A spin-coated wafer is secured to the rheometer's Peltier heater (heating rate of ∼90 °C/min). Polydimethylsiloxane (PDMS) oil (room-temperature kinematic viscosity of 1.0×10^6 cSt, United Chemical Technologies or Gelest) is placed between the thin film and a parallel plate fixture mounted on the rheometer head.[18] This

10.1021/ma0713310 CCC: $37.00
Published on Web 09/11/2007

assembly is then heated to the desired temperature before the rheometer head is rotated at a constant stress. After shearing, the temperature is decreased to ambient and the oil removed from the film by "sponging" with a cross-linked PDMS pad. The parallel plate fixture allows for a continuous gradient in stress along the radial direction in the sheared film

$$\tau = \eta\dot{\gamma} = \frac{r}{R}\tau_{\max} \tag{1}$$

where $\dot{\gamma}$ is the shear rate within the PDMS oil, R is the radius of the shearing plate, r is the in-plane distance from the rotation axis to the edge of the shearing plate, and $\tau_{\max}$ is the stress at the edge of the shearing plate. Equation 1 assumes that the PDMS oil is Newtonian, which we confirmed accurate to within 10% up to the largest $\tau_{\max}$ employed here (3200 Pa, at 85 °C).

Imaging and Analysis. The thin films are imaged using a Digital Instruments Dimension 3000 Atomic Force Microscope in tapping Mode. At room temperature, the elastic modulus of the two phases is different enough to be detected in phase mode without destruction of the film. Quantitative analysis of these images is done using customized software written in Interactive Data Language (IDL). Each image is stretched to correct for piezo and thermal drifting during data acquisition[23] and Fourier filtered with an annulus convoluted with a Gaussian blur to remove high- and low-frequency noise. The position of each sphere is determined using a particle finding algorithm.[24] Using the coordinates of the centers of the spheres a Delaunay triangulation is done to find nearest neighbors; this triangulation easily locates disclinations, characterized by having a number of nearest neighbors different from six (typically five or seven, occasionally four or eight). Neighboring disclinations of opposite sign (or charge) are defined to be dislocations,[25] which are found using an algorithm that minimizes the number of isolated disclinations. By knowing where each sphere is located along with its nearest neighbors, the orientation of each bond vector can easily be calculated. The orientational order parameter is defined as

$$\psi_6 = \langle\cos(6(\theta - \theta_0))\rangle = \langle\cos(6\delta\theta)\rangle \tag{2}$$

where θ is the orientation of the bond vector, θ_0 is the shear direction, and the factor of 6 is required for the 6-fold symmetry of the hexagonal lattice. The average is taken over all bond vectors in the image. A value of $\psi_6 = 1$ corresponds to all bond vectors oriented along the shear direction (modulo 60°), -1 corresponds to all bond vectors oriented 30° from the shear direction, and 0 is expected for a random global orientation of the bond vectors. The position of the rheometer's rotation axis in the plane of the film is determined from scratches made around the edge of the shearing plate, whose positions in the AFM images are fit to a circle. The shear direction θ_0 is then determined from the location where the image was acquired relative to the rotation axis.

Results and Discussion

Previous work from our group has quantified the relationship between the orientational order parameter ψ_6 and the shear stress for this sphere-forming PS-PEP diblock and presented a phenomenological model to explain the results.[18] The essential feature of the model is that the energetic coupling between layers, for grains oriented such that $\delta\theta \neq 0$, causes a destabilization of the microphase-separated state; in other words, grains are destabilized by an amount related to $\delta\theta$ and ultimately "melted". These regions subsequently "recrystallize" into orientations better aligned with the shear. To achieve any reorganization of the film, a threshold stress must be exceeded, which corresponds to the stress required for the most misaligned grains ($\delta\theta = 30°$) to melt at the shearing temperature T ($< T_{ODT}$). As the stress is increased or the shearing temperature increased toward T_{ODT}, a larger fraction of the grains in the initial distribution are melted by the shear.

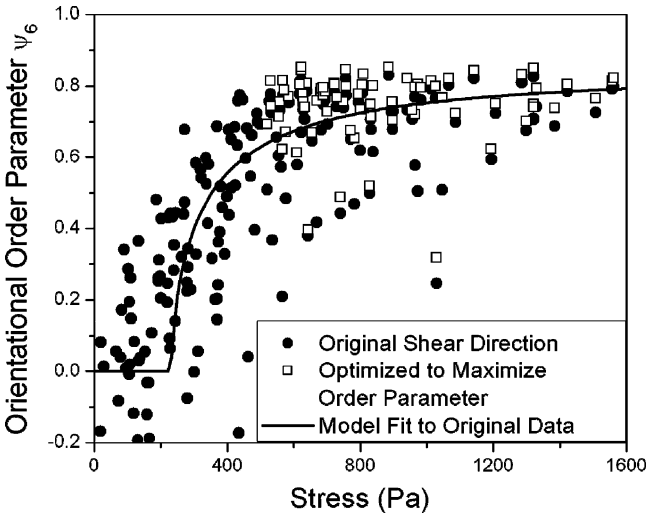

Figure 1. Dependence of orientational order parameter ψ_6 on shear stress for PS-PEP films, containing three layers of spheres, sheared at 85 °C for 30+ min. Filled circles were calculated with the shear direction θ_0 determined independently; open squares were calculated by allowing θ_0 to float for each image to maximize ψ_6. The continuous curve is a fit to the model described in ref 18.

Figure 1 shows the relationship between ψ_6 and the applied shear stress after extended shearing at 85 °C (36 °C below the bulk T_{ODT} for this diblock). Extensive new data are added to those already presented in ref 18 along with a fit to the recrystallization model. At low stress values, the order parameter scatters about zero; the large scatter results from the grain size of annealed PS-PEP[7] being comparable to the size of the AFM image. As the stress increases, ψ_6 rises and eventually plateaus at a value less than 1, suggesting imperfect alignment even at very high stresses. Our principal focus in the present work is elucidating and quantifying the factors which lead to this limiting value of the orientational order parameter, but we begin with a discussion of the behavior at lower stresses.

Stresses Below the Plateau Region. Nearly all of the defects present in the images are dislocations; only a very few isolated disclinations are present at some of the intersections of three grain boundary lines.[26] This is expected since the strain energies of isolated disclinations are high compared to dislocations.[27] As shown in Figure 2a and b, at stresses below the plateau region, dislocations are found almost exclusively on grain boundaries with a few isolated dislocations located within the grains. At the lowest stresses (Figure 2b), grains of all orientations are present; at higher values of stress but still below the plateau region, the grains at the largest mismatch to the shear direction are eliminated (Figure 2c).

Analyzing the bond vector orientation distribution reveals how grain boundaries are annihilated as the stress is increased. Figure 3 shows the distributions averaged over 10−20 images within the stress ranges shown. Below the threshold stress (σ_{thresh}, defined as the minimal stress required to induce observable alignment in the thin films, 230 Pa from the model fit shown in Figure 1) the distribution is relatively flat, as expected for a polygranular film. As the stress is increased above σ_{thresh}, the most misaligned grains (at ±30° relative to the shear direction) are preferentially destroyed, in accordance with our previously described model.[18]

At higher stresses, Figure 3 shows the progressive destruction of grains of intermediate misalignment (±10−20°). At the

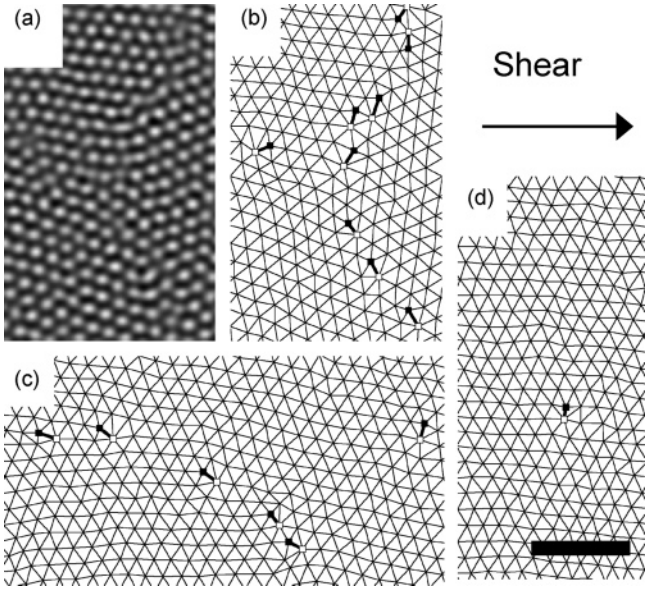

Figure 2. Effect of shear on grain boundaries; scale bar = 150 nm for all panels. (a) AFM image at low stress (230 Pa). (b) Delaunay triangulation of the same AFM image showing that dislocations reside almost exclusively on grain boundaries. Grains have the full range of orientations with respect to the shear direction. Dislocations are indicated by bold line segments connecting a five-coordinate sphere (filled square) with a neighboring seven-coordinate sphere (open square). (c) At moderate stresses (430 Pa) dislocations still form grain boundaries, but the grains at the greatest mismatch to the shear direction have been eliminated. (d) At high stresses (1320 Pa), in the plateau region where ψ_6 is independent of stress, no grain boundaries remain; only isolated dislocations are present.

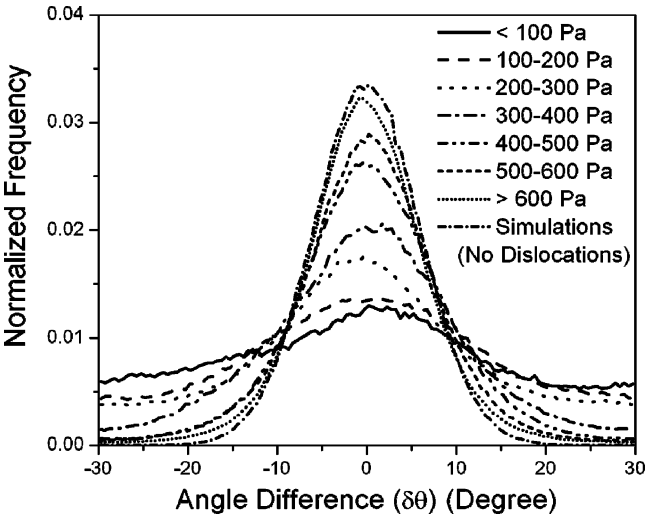

Figure 3. Distribution of bond vector orientations with respect to the shear direction (modulo 60°), as a function of applied shear stress. The relatively flat distribution measured at low stresses becomes peaked around $\delta\theta = 0$ as stress is increased. The curve labeled "simulations" corresponds to the distribution calculated for a defect-free aligned lattice with Gaussian noise in the sphere positions.

highest stresses, only isolated dislocations remain; no observable grain boundaries are evident (Figure 2d). However, at the highest stresses the measured bond vector orientation distribution (Figure 3) does not appear to narrow toward a delta function at $\delta\theta = 0$, as expected for perfect alignment, but rather limits toward a bell-shaped distribution with a width at half-maximum of approximately ±7°. This limit mirrors that in ψ_6 at high stresses (Figure 1), both of which are addressed next.

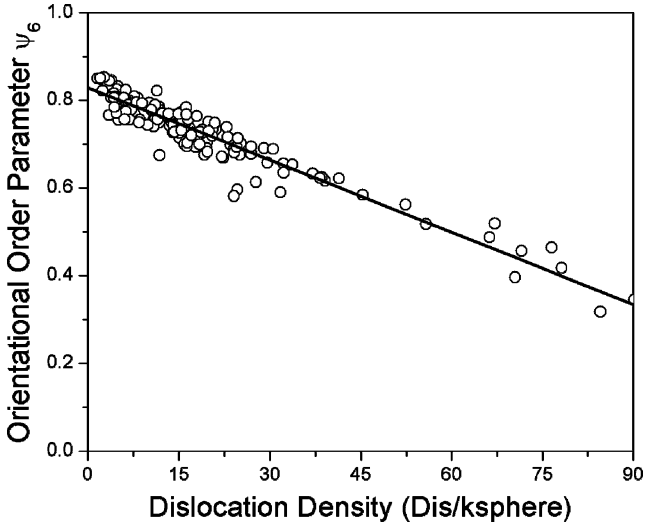

Figure 4. Orientational order parameter as a function of dislocation density for PS-PEP films, containing three layers of spheres, sheared at 65−95 °C for 5−120 min. Only data in the plateau region (ψ_6 independent of stress, no grain boundaries, isolated dislocations only) are shown.

Stresses in the Plateau Region. The orientation of the bond vectors is calculated with respect to the shear direction θ_0, so even for a perfectly aligned sample, any error in determining θ_0 would yield $\psi_6 < 1$. Similarly, since the orientation distributions in Figure 3 are averages over many images, random errors in θ_0 for each image would broaden the distribution. To assess this possibility, θ_0 for each image was adjusted to match the average bond vector orientation (modulo 60°) and ψ_6 was recalculated. Figure 1 also shows these recalculated ψ_6 values, which do not differ substantially from those calculated using the independently measured θ_0; indeed, the two values of θ_0 were within 2° in all cases. The breadth of the bond vector orientation distribution (as in Figure 3) is not observably changed by this recalculation either. Thus, the apparent limits on orientational order are not an artifact of imperfectly determining the shear direction.

Along the plateau region isolated dislocations are the only topological defects in the samples. Figure 4 plots ψ_6 vs dislocation density (number of dislocations per 1000 spheres) for these high-stress specimens; to maximize the volume of data, points corresponding to shearing temperatures ranging from 65 to 95 °C are combined. As the temperature is reduced (further from T_{ODT}), larger values of stress are required to access the plateau region, but no systematic difference was discernible in the ψ_6 vs dislocation density relationship for specimens sheared at different temperatures within this high-stress region. As illustrated in Figure 4, ψ_6 is apparently linear in dislocation density with a slope of −0.0055 kspheres/dislocation. Extrapolation to the *x* intercept gives a value for the dislocation density needed to completely destroy the orientational order: 140 dislocations per 1000 spheres, meaning that when 1 dislocation is present for every 7 spheres, no bond vector orientational order would be expected. Equally interesting, the apparent *y* intercept of this line is not at the expected value of unity but rather at $\psi_6 = 0.83$, implying that even in the absence of any dislocations only finite orientational order is achievable. We address this apparent limitation in the following section.

Sphere Positional Uncertainty. ψ_6 is an average over the orientations of all bond vectors, which are the line segments connecting adjacent spheres. Any imprecision in locating the

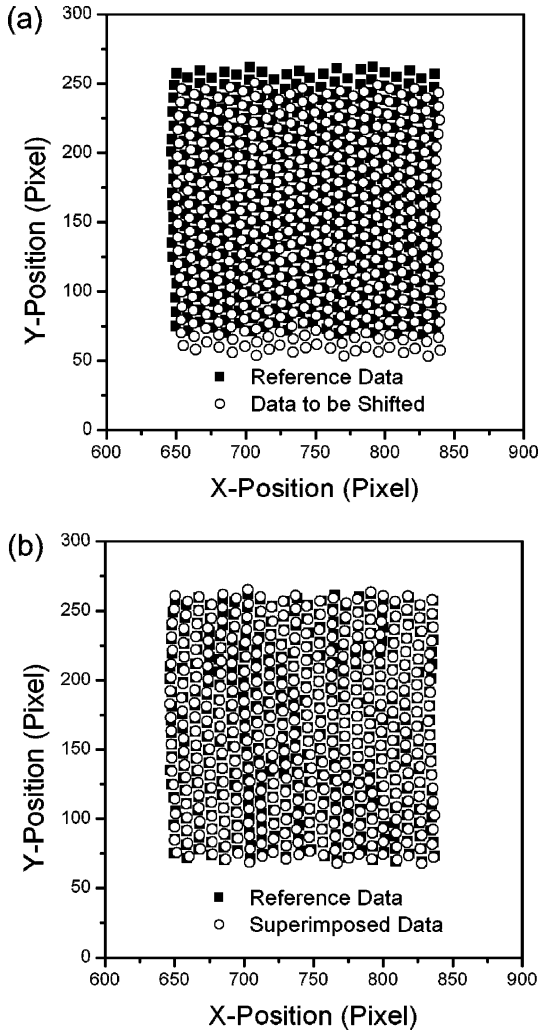

Figure 5. Matching sphere positions in two AFM images of the same region of the film (pixel-to-pixel distance = 2.4 nm). (a) Symbols show original positions of spheres. (b) Sphere positions after rigid body translation and rotation. Remaining deviations in positions between black and white points can be described by Gaussian random noise with a standard deviation of 7.5% of the intersphere spacing.

centers of the spheres thus directly impacts ψ_6. To quantify the precision with which the center of each sphere can be located by our AFM imaging and analysis protocols, the same area of a film was imaged multiple times. All permutations of imaging sequence were employed (collecting the data during trace or retrace; slow scan top to bottom or bottom to top; fast scan vertical instead of horizontal, with the corresponding swap of the slow scan direction), for a total of eight independent but nominally identical images. These images were then cropped to a smaller area (475 nm × 475 nm), free from dislocations; selection of a smaller area minimizes residual piezo drift (after overall correction on the full image). Different images were superimposed by rigid-body translation and rotation (<1°) as illustrated in Figure 5. The uncertainty in sphere positions was then calculated from the differences between the positions of all the spheres in the *x* and *y* directions. The standard deviation in each direction was found to be 7.5% of the intersphere spacing of 24.5 nm with no significant dependence on the choice of imaging sequence. The principal source of this uncertainty appears to be amplitude noise in the images; since each sphere spans only five pixels in the AFM image, any pixel intensity fluctuation can impact determination of the sphere position, which is the intensity centroid.

To check the impact that this level of uncertainty in the sphere position has on ψ_6 and the bond vector orientation distribution, we numerically constructed a perfect hexagonal lattice and added random noise to both the *x* and *y* sphere coordinates following a Gaussian distribution with a standard deviation of 7.5% of the lattice spacing. For this simulated lattice, $\psi_6 = 0.85$, in good agreement with the extrapolated *y* intercept in Figure 4. For this simulated noisy lattice we also calculated the bond vector orientation distribution, which is plotted in Figure 3 and agrees quite well with the experimental data at high stresses. These results suggest that the observed limitation on orientational order at low dislocation densities is in fact only apparent, an artifact of the precision with which the centers of the spheres can be located. Any actual Debye−Waller-like deviation of the spheres from their lattice positions is much smaller than our imaging resolution, and the actual order of the lattice at low dislocation densities is much better than the data in Figures 1 and 3 suggest.

Isolated Dislocations: Density and Orientation. First, one may ask why the range of dislocation densities (Figure 4) is so large—more than an order of magnitude variation—in nominally identical shear-aligned films. Each data point in Figure 4 represents an average over a full-size AFM image, which contains approximately 10 000 spheres (10 kspheres), so the variation is much greater than can be attributed to the finite image size. The vast majority of the data points in Figure 4 are clustered below 30 dis/ksphere; those images revealing higher dislocation densities were not randomly distributed across the entire collection but instead came from a few particular specimens that showed uniformly higher dislocation densities. We believe that these variations are caused by slight differences in film thickness from specimen to specimen. Earlier work on shear alignment of this same PS-PEP diblock with a cross-linked PDMS pad, on films having a thickness gradient, demonstrated that the films needed to be within ±1 nm of the thickness corresponding to an integral number of layers of spherical domains for shear alignment to be effective.[17] While such tight control of film thickness appears critical for achieving the best-ordered films, slight variations from the optimal thickness are fortuitous in the present case as they allow us to access a broad range of isolated dislocation densities.

Next, we address the orientation of these isolated dislocations. In a two-dimensional hexagonal lattice these are formed by adjacent disclinations of opposite sign. Each dislocation adds two additional lines of spheres to the lattice and has a Burgers vector that is perpendicular to the bond connecting the disclinations (see Figure 6). This Burgers vector should lie along a bond vector, so that the orientation of the dislocation (defined as the direction of the bond vector connecting the disclinations) is −150°, −90°, −30°, 30°, 90°, or 150° to neighboring bond vectors. Thus, in an aligned perfect lattice, isolated dislocations should be oriented −150°, −90°, −30°, 30°, 90°, or 150° to the shear direction with delta-function distributions. Since the calculation of $\delta\theta$ between the dislocation and shear directions is also subject to the sphere positional uncertainty discussed above, these delta functions are broadened (standard deviation of 7.5%); this expected distribution of dislocation orientations is plotted in Figure 7 along with the observed distribution. Experimentally, dislocations are preferentially oriented perpendicular to the shear direction ($\delta\theta = \pm 90°$); the areas of the two peaks at ±90° are identical to within 1%.

Figure 8 presents a qualitative argument for the origin of this preferred dislocation orientation by showing the shear-induced

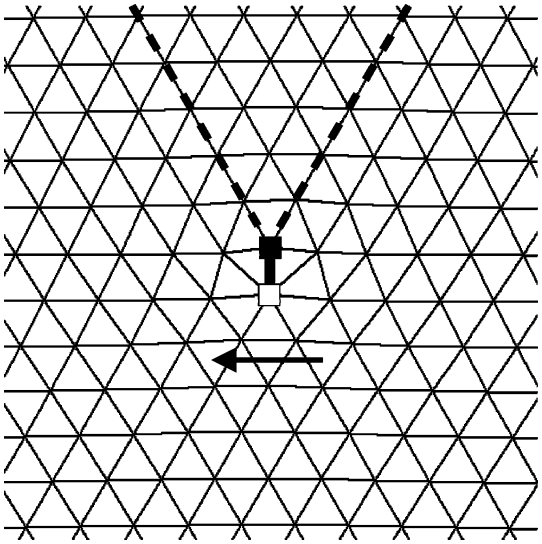

Figure 6. Delaunay triangulation of spheres around a dislocation. In a hexagonal lattice a dislocation produces two additional rows of spheres shown with dashed lines. The Burgers vector of the dislocation has a magnitude of one lattice spacing and an orientation shown by the arrow.

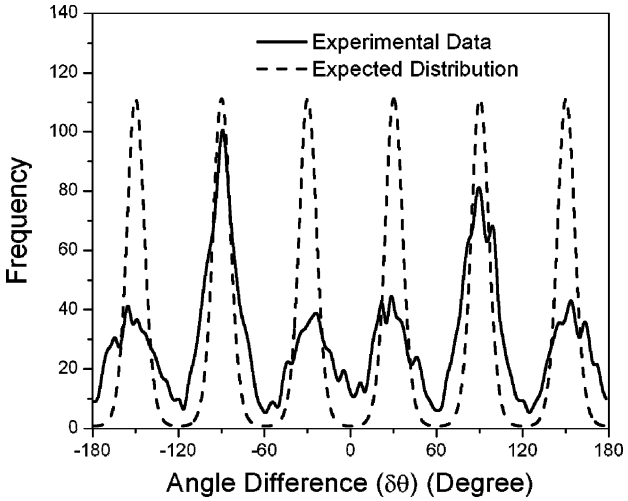

Figure 7. Bond vector orientation distribution in a shear-aligned film. Dashed line: expected distribution assuming equal probabilities for dislocations to have their Burgers vector lying along any lattice direction. Solid line: experimentally measured distribution, showing a preference for dislocations to orient perpendicular to the shear direction ($\delta\theta = \pm 90°$).

relative movement of spheres in a simple bilayer sample. If a dislocation is oriented normal to the shear direction there is no restriction to sliding of the layers of spheres past one another. If the orientation differs from $\pm 90°$ the shear exerts a force on the dislocation, which represents an energetic penalty that disfavors (but does not eliminate) dislocations oriented at $\pm 30°$ and $\pm$ 150° to the shear direction. Alternatively, it is interesting to note that a Frank−Read source[28] terminating in two dislocations at the upper surface also has the correct Burgers vector to facilitate sliding between layers.

Elastic Continuum Simulations. To model the effect of a dislocation on the bond vector orientation we treat the lattice as an elastic continuum deformed to create an edge dislocation, forming a broken annulus, as shown in Figure 9. The equations

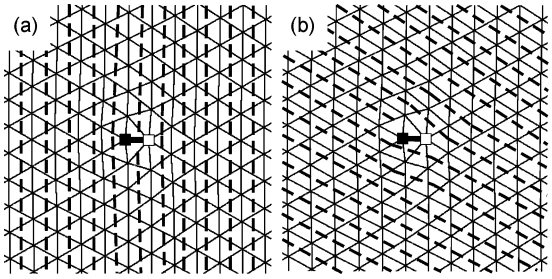

Figure 8. Schematic of how the layers of spheres in a simple bilayer film slide past one another for two different orientations of the shear direction relative to a dislocation. Thin solid lines indicate the Delaunay triangulation of the top layer of spheres, while dashed lines indicate the trajectory of the bottom layer of spheres. (a) Shear direction vertical, so the dislocation is normal to the shear direction. (b) Shear direction diagonal, oriented 30° from the dislocation.

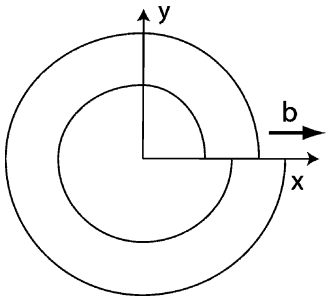

Figure 9. Schematic of in-plane displacements induced by an edge dislocation in an elastic continuum, viewed along the *z* direction.

that describe the displacements from the ideal lattice positions are, to first order[29]

$$u_x = \frac{b}{2\pi}\left(\tan^{-1}(y/x) + \frac{xy}{2(1-\upsilon)(x^2+y^2)}\right) \quad (3)$$

$$u_y = \frac{b}{2\pi}\left(\frac{-(1-2\upsilon)}{4(1-\upsilon)}\log(x^2+y^2) + \frac{y^2}{2(1-\upsilon)(x^2+y^2)}\right) \quad (4)$$

where u_x and u_y are the displacements in x and y and υ is Poisson's ratio. We choose the bulk value of $\upsilon = 1/2$ for an incompressible material to represent our trilayer films; eqs 3 and 4 are predicated on no deformation in the third (z) direction (since they model an edge dislocation in a 3D crystal), so the thinness (finite z dimension) of our films should have no influence on the x and y displacements to first order. These equations have a singularity at $x = y = 0$, and eq 4 diverges as x or y approaches infinity, but these equations are valid in a finite region outside the dislocation core. We assume that the dislocation core is small enough that the positional shifts to all spheres in the hexagonal lattice can be described by the equations above. To maximize the size of the dislocation core but not have it cover any spheres, the center of the dislocation is stationed over the center of a bond. The x axis in Figure 9 is oriented along a bond direction so that only the six orientations of dislocations are possible; displacements caused by neighboring dislocations are simply summed. Dislocations are inserted at randomly selected positions in the lattice and randomly assigned one of the six allowable orientations. If the dislocation to be inserted would have its x axis intersect the center of another dislocation, another dislocation was randomly generated instead, so these simulations are accurate only in the low dislocation density limit.

Figure 10 shows ψ_6 calculated from these simulated lattices (top cluster of points). Lattices were also simulated wherein

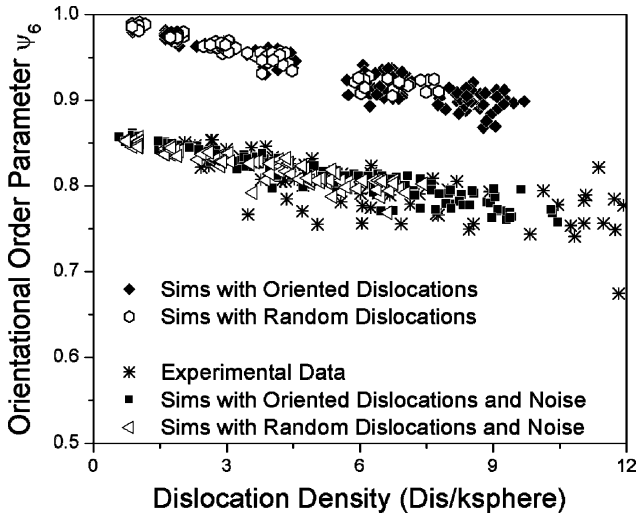

Figure 10. Comparison of experimental orientational order parameter (ψ_6) with that calculated using the elastic continuum model. Top band of points are for noise-free lattices calculated with preferentially oriented dislocations (filled symbols) and randomly oriented dislocations (open symbols). Lower band of points include experimental values along with simulations assuming a sphere positional uncertainty of 7.5% (standard deviation) of the intersphere spacing.

the dislocations were all oriented ±90° to the shear direction to represent the limiting case of the preferred dislocation orientation seen experimentally in Figure 7. Over the range of dislocation densities simulated there is no difference between ψ_6 for randomly oriented vs preferentially oriented dislocations. Both data sets follow an apparently linear dependence with a slope of −0.0114 ksphere/dislocation. Using a slightly smaller value of Poisson's ratio ($\upsilon = 0.37$), as suggested by the theoretical work of Tyler and Morse,[30] produced very similar results with a slope of −0.0101 ksphere/dislocation. Next, Gaussian random noise (standard deviation of 7.5% of the intersphere spacing) was added to the *x* and *y* coordinates of the sphere positions in the elastically deformed lattice to mimic the imaging and analysis uncertainty. This added noise essentially rescales the calculated ψ_6 curve by a factor of 0.85, as shown in Figure 10; comparison of these calculations with the experimental ψ_6 data, also plotted in Figure 10, reveals excellent quantitative agreement. Both follow essentially linear correlations with best-fit slopes of −0.0098 ksphere/dislocation for the simulated data and −0.0096 ksphere/dislocation for the experimental data within this dislocation density range. The difference in slope here vs Figure 4 reflects the narrower range of dislocation densities in Figure 10 and implies that the actual ψ_6 vs dislocation density plot is mildly concave upward. This curvature leads to a slight increase in the intercept when only the data at low dislocation densities is fit, to $\psi_6 = 0.86$, again in good quantitative agreement with the value of 0.85 attributable solely to uncertainty in the sphere positions.

The quantitative agreement between the model and experiment is somewhat surprising given the model's simplicity. For example, Hammond et al. have shown that the stresses around a dislocation cause the spheres to stretch or compress depending on the charge of the disclination,[31] but such effects are completely absent in this elastic continuum model. Since ψ_6 is an average over the entire image, local deformations near the dislocation evidently have little effect, at least at the low dislocation densities relevant for well-aligned films.

Conclusions

In thin films of sphere-forming block copolymers orientational order is principally governed by the density and distribution of dislocations. At low stresses, nearly all dislocations are located on grain boundaries. As the stress is increased, grains at the greatest mismatch to the shear direction are annihilated first. Once the stress reaches a sufficient level, the orientational order parameter ψ_6 no longer shows a systematic dependence on shear stress. In this region, ψ_6 is instead dictated by the density of isolated dislocations within the film; ψ_6 decreases roughly linearly with dislocation density. However, even in the zero-dislocation limit, ψ_6 asymptotes below unity, near 0.85. This apparent limit results from uncertainty in the positions of the spheres as determined by AFM imaging and analysis; independent measurements of this uncertainty agree quantitatively with the apparent asymptotes in ψ_6 and bond vector orientation distribution. Since this uncertainty arises in the imaging and analysis rather than being present in the lattice, an important conclusion from this work is that orientational order in these shear-aligned films is limited only by the residual isolated dislocations. The isolated dislocations show a preferred direction perpendicular to the shear, an orientation which facilitates the sliding of layers of spheres past one another. We model the system as an elastic continuum with a sphere positional uncertainty matching that in the experiment. This simple model agrees quantitatively with the experimental measurements of ψ_6 vs dislocation density in the high-stress region.

Acknowledgment. This work was supported by the National Science Foundation (MRSEC Program) through the Princeton Center for Complex Materials (DMR-0213706). The authors thank Professor Daniel A. Vega (Universidad Nacional del Sur) for helpful discussions and assistance with the simulations.

References and Notes

(1) Hamley, I. W. *The Physics of Block Copolymers*; Oxford University Press: Oxford, 1998.
(2) Bates, F. S.; Frederickson, G. H. *Phys. Today* **1999**, *52*, 32−38.
(3) Segalman, R. A. *Mater. Sci. Eng., R* **2005**, *48*, 191−226.
(4) Trawick, M.; Angelescu, D.; Chaikin, P.; Register, R. In *Nanolithography and Patterning Techniques in Microelectronics*; Bucknall, D. G., Ed.; Woodhead Publishing: Cambridge, 2005; pp 1−38.
(5) Amundson, K.; Helfand, E.; Patel, S. S.; Quan, X.; Smith, S. D. *Macromolecules* **1992**, *25*, 1935−1940.
(6) Newstein, M. C.; Garetz, B. A.; Dai, H. J.; Balsara, N. P. *Macromolecules* **1995**, *28*, 4587−4597.
(7) Harrison, C.; Angelescu, D. E.; Trawick, M.; Cheng, Z.; Huse, D. A.; Chaikin, P. M.; Vega, D. A.; Sebastian, J. M.; Register, R. A.; Adamson, D. H. *Europhys. Lett.* **2004**, *67*, 800−806.
(8) Segalman, R. A.; Yokoyama, H.; Kramer, E. J. *Adv. Mater.* **2001**, *13*, 1152−1155.
(9) Naito, K.; Hieda, H.; Sakurai, M.; Kamata, Y.; Asakawa, K. *IEEE Trans. Mag.* **2002**, *38*, 1949−1951.
(10) Cheng, J. Y.; Ross, C. A.; Thomas, E. L.; Smith, H. I.; Vancso, G. J. *Adv. Mater*. **2003**, *15*, 1599−1602.
(11) Chuang, V. P.; Cheng, J. Y.; Savas, T. A.; Ross, C. A. *Nano Lett*. **2006**, *6*, 2332−2337.
(12) Kim, S. H.; Misner, M. J.; Xu, T.; Kimura, M.; Russell, T. P. *Adv. Mater*. **2004**, *16*, 226−231.
(13) Black, C. T.; Bezencenet, O. *IEEE Trans. Nanotechnol*. **2004**, *3*, 412−415.
(14) Xiao, S. G.; Yang, X. M.; Edwards, E. W.; La, Y.-H.; Nealey, P. F. *Nanotechnology* **2005**, *16*, S324−S329.
(15) Stein, G. E.; Kramer, E. J.; Li, X.; Wang, J. *Phys. Rev. Lett.* **2007**, *98*, 086101.
(16) Angelescu, D. E.; Waller, J. H.; Adamson, D. H.; Deshpande, P.; Chou, S. Y.; Register, R. A.; Chaikin, P. M. *Adv. Mater.* **2004**, *16*, 1736−1740.
(17) Angelescu, D. E.; Waller, J. H.; Register, R. A.; Chaikin, P. M. *Adv. Mater*. **2005**, *17*, 1878−1881.

(18) Wu, M. W.; Register, R. A.; Chaikin, P. M. *Phys. Rev. E* **2006**, *74*, 040801.
(19) Pelletier, V.; Adamson, D. H.; Register, R. A.; Chaikin, P. M. *Appl. Phys. Lett.* **2007**, *90*, 163105.
(20) Sebastian, J. M.; Lai, C.; Graessley, W. W.; Register, R. A. *Macromolecules* **2002**, *35*, 2707−2713.
(21) Adams, J. L.; Quiram, D. J.; Graessley, W. W.; Register, R. A. *Macromolecules* **1998**, *31*, 201−204.
(22) Stein, G. E.; Kramer, E. J.; Li, X.; Wang J. *Macromolecules* **2007**, *40*, 2453−2460.
(23) Trawick, M. L.; Megens, M.; Harrison, C.; Angelescu, D. E.; Vega, D. A.; Chaikin, P. M.; Register, R. A.; Adamson, D. H. *Scanning* **2003**, *25*, 25−33.
(24) Crocker, J. C.; Grier, D. G. *J. Colloid Interface Sci.* **1996**, *179*, 298−310.
(25) Chaikin, P. M.; Lubensky, T. C. In *Principles of Condensed Matter Physics*; Cambridge: Cambridge University Press, 1995; p 517.
(26) Gomez, L. R.; Valles, E. M.; Vega, D. A. *Phys. Rev. Lett.* **2006**, *97*, 188302.
(27) Vega, D. A.; Harrison, C. K.; Angelescu, D. E.; Trawick, M. L.; Huse, D. A.; Chaikin, P. M.; Register, R. A. *Phys. Rev. E* **2005**, *71*, 061803.
(28) Frank, F. C.; Read, W. T., Jr. *Phys. Rev.* **1950**, *79*, 722−723.
(29) Kelly, A.; Groves, G. W.; Kidd, P. *Crystallography and Crystal Defects*, Rev. Ed.; John Wiley & Sons, Ltd.: Chichester, 2000; p 234.
(30) Tyler, C. A.; Morse, D. C. *Macromolecules* **2003**, *36*, 3764−3774.
(31) Hammond, M. R.; Sides, S. W.; Fredrickson, G. H.; Kramer, E. J.; Ruokolainen, J.; Hahn, S. F. *Macromolecules* **2003**, *36*, 8712−8716.

MA0713310